

Two-Phonon Quantum Coherences in Indium Antimonide Studied by Nonlinear Two-Dimensional Terahertz Spectroscopy

Carmine Somma, Giulia Folpini, Klaus Reimann, Michael Woerner,^{*} and Thomas Elsaesser
Max-Born-Institut für Nichtlineare Optik und Kurzzeitspektroskopie, 12489 Berlin, Germany
(Received 25 January 2016; published 28 April 2016)

We report the first observation of two-phonon quantum coherences in a semiconductor. Two-dimensional terahertz (THz) spectra recorded with a sequence of three THz pulses display strong two-phonon signals, clearly distinguished from signals due to interband two-photon absorption and electron tunneling. The two-phonon coherences originate from impulsive off-resonant excitation in the nonperturbative regime of light-matter interaction. A theoretical analysis provides the relevant Liouville pathways, showing that nonlinear interactions using the large interband dipole moment generate stronger two-phonon excitations than linear interactions.

DOI: [10.1103/PhysRevLett.116.177401](https://doi.org/10.1103/PhysRevLett.116.177401)

Phase-coherent superpositions of the wave functions of different quantum states represent a fundamental elementary excitation of matter. In a basic generation scheme, an optical field interacting resonantly with the transition dipole between two levels induces a quantum coherence connected with a coherent optical polarization. Such one-quantum coherences have been generated, optically manipulated, and read out on both electronic and vibrational transitions in a wide range of condensed-matter systems [1–6]. Decoherence due to nonadiabatic couplings and/or scattering processes determines their temporal evolution in the subpico- to picosecond time domain, requiring ultrashort optical pulses for mapping coherent dynamics in nonlinear time-resolved spectroscopy [7–11]. Decoherence of one-photon excitations has been the subject of extensive theoretical work, which has allowed for identifying the underlying interaction mechanisms [12–14].

Much less is known about two-quantum coherences, in which the phases of two coupled excitations are locked. The optical excitation of two-quantum coherences is inherently nonresonant. Both linear and nonlinear generation schemes exist, the relative efficiency of which has remained unknown, as have the dynamics of two-quantum coherences. Prototypical two-quantum excitations are phonon combination tones in crystalline solids, which have been studied by stationary linear absorption and Raman spectroscopies. The phonon system has also attracted considerable interest from the new field of quantum phononics, where nonclassical states such as squeezed and entangled phonons have been investigated [15–19]. In the narrow-gap material InSb, which is a prototypical III–V semiconductor, different second-order bands of transverse acoustic as well as transverse and longitudinal optical phonons have been observed [20,21]. Second-order Raman data have allowed for determining the related electron–two-phonon deformation potentials [22]. Coherent dynamics, however, have not yet been studied.

In this Letter, we report the first time-resolved study of two-phonon coherences. We apply a novel method of nonlinear two-dimensional (2D) terahertz (THz) spectroscopy to measure the coherent THz emission of two-phonon excitations in bulk InSb in amplitude and phase and identify the relevant nonlinear interaction mechanisms.

Our experiments are based on phase-resolved 2D collinear THz spectroscopy [23,24]. In contrast to all previous 2D THz studies, we implement a sequence of three pulses interacting with the sample [Fig. 1(b)]. The phase-locked pulses *A* and *B* are separated by the coherence time τ , while pulse *C* is delayed by the waiting time T_w relative to pulse *B*. The pulses incident on and transmitted through the sample and the THz emission from the sample are detected by phase-resolved electro-optic sampling [25], giving the THz electric fields as a function of the real time t . THz pulses with a center frequency of 20 THz, a bandwidth of 6 THz, and pulse lengths between 100 and 200 fs are generated by optical rectification of 800 nm input pulses in three separate GaSe crystals (thickness, 100 μm). The 25 fs pulses at 800 nm and a 1 kHz repetition rate are generated in two multipass Ti:sapphire amplifiers synchronously seeded by the output of a Ti:sapphire oscillator. A 10- μm -thick (110)-oriented ZnTe serves for electro-optic sampling with 12 fs pulses from the Ti:sapphire oscillator [26].

With three pulses incident on the sample, the signal contains the linear response and one-, two-, and three-pulse nonlinear responses. To separate the pure three-pulse nonlinear response, we use three mechanical choppers synchronized to one half, one quarter, and one eighth of the 1 kHz repetition rate of the amplifiers. In this way, seven transients are determined, one when all three pulses *ABC* interact with the sample, three for the pairs *AB*, *BC*, and *CA*, and three for the single pulses *A*, *B*, and *C*. From these transients, the pure three-pulse nonlinear field emitted by the sample is derived as

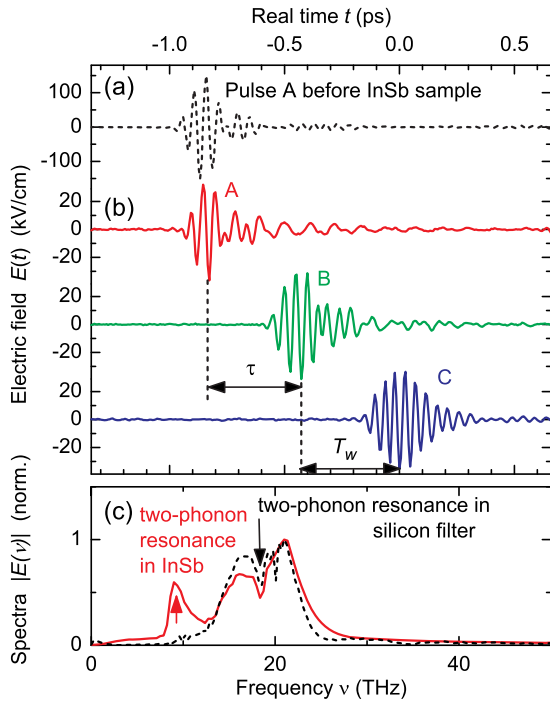


FIG. 1. (a) Incident THz electric field transient A as a function of real time. (b) Electric field transients A , B , and C transmitted through the InSb sample. τ is the coherence time, T_w the waiting time in the 2D experiment. (c) Incident (dashed line) and transmitted (solid line) spectra. The sharp dips at 18 THz stem from linear two-phonon absorption in the silicon filters blocking the 800 nm pulses used for generating the THz pulses. The peak around 10 THz originates from the impulsively excited two-phonon coherence in InSb.

$$E_{\text{NL}}(\tau, T_w, t) = E_{ABC}(\tau, T_w, t) - E_{AB}(\tau, T_w, t) - E_{BC}(T_w, t) - E_{CA}(\tau, T_w, t) + E_A(\tau, T_w, t) + E_B(T_w, t) + E_C(t). \quad (1)$$

A 2D Fourier transform of $E_{\text{NL}}(\tau, T_w, t)$ along τ and t generates the frequency-domain signal $E_{\text{NL}}(\nu_\tau, \nu_t)$ as a function of the excitation frequency ν_τ and the detection frequency ν_t .

The semiconductor sample studied at room temperature is a 70- μm -thick (100)-oriented InSb single crystal with a low n -type doping ($n \leq 10^{16} \text{ cm}^{-3}$). The fundamental band gap of $E_g = 0.17 \text{ eV}$ [27,28] corresponds to a frequency of $\nu_{\text{THz}} = E_g/h = 41 \text{ THz}$. Around 10 THz, the InSb crystal displays several two-phonon absorption lines [20]. It is important to note that the incident 20 THz pulses are nonresonant with respect to both the band gap and the two-phonon lines.

THz transients are shown in Figs. 1(a) and 1(b), where the electric field is plotted as a function of the real time t . Figure 1(a) shows the pulse A before interaction with the sample, Fig. 1(b) the pulses A , B , and C transmitted through the sample with their mutual delays τ and T_w .

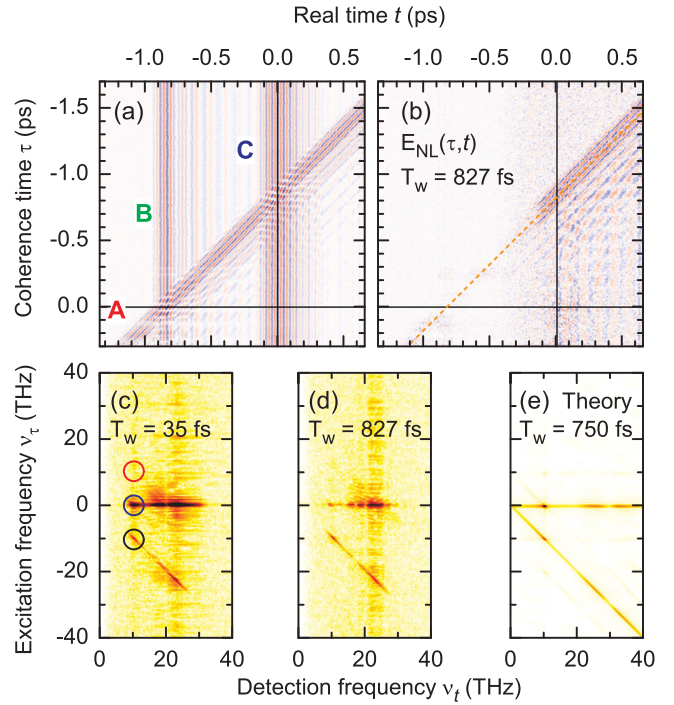


FIG. 2. Two-dimensional THz spectroscopy on InSb. (a) Contour plot of the electric field transient $E_{ABC}(\tau, T_w, t)$ transmitted through the InSb sample as a function of the coherence time τ and the real time t . (b) Nonlinear signal $E_{\text{NL}}(\tau, T_w, t)$ according to Eq. (1) for a waiting time $T_w = 827 \text{ fs}$. The dashed line indicates the center of pulse A . (c),(d) Contour plot of the amplitude $|E_{\text{NL}}(\nu_\tau, \nu_t)|$, the 2D Fourier transform of $E_{\text{NL}}(\tau, T_w, t)$, for two waiting times T_w . The colored circles indicate the position of the two-phonon signals in the 2D frequency space. (e) Theoretical 2D signal calculated for a waiting time $T_w = 750 \text{ fs}$.

The real time $t = 0$ is set at the maximum of pulse C . In contrast to the incident pulse, the transmitted pulse A shows an additional oscillating field component between $t = -0.6 \text{ ps}$ and $t = 0 \text{ ps}$ which is radiated by the sample and decays on a time scale of 1 ps. A Fourier transform of the time-dependent fields gives the spectra in Fig. 1(c). The additional time-dependent field component in the transmitted pulse A gives rise to the pronounced peak around 10 THz, i.e., at the two-phonon resonance of InSb.

In Fig. 2, we present results of the three-pulse 2D experiments. Figure 2(a) shows a contour plot of the sum of the electric field transients $E_A(\tau, T_w, t) + E_B(T_w, t) + E_C(t)$ transmitted through the InSb sample as a function of the coherence time τ and the real time t for a waiting time $T_w = 827 \text{ fs}$. All contour plots are normalized to their respective maximum signal. Using Eq. (1), we calculated the time-dependent nonlinear signal $E_{\text{NL}}(\tau, T_w, t)$ shown in Fig. 2(b). In accordance with causality, a nonvanishing $E_{\text{NL}}(\tau, T_w, t)$ is observed only after the last pulse in the timing sequence. The orange dashed line indicates the center of pulse A , which intersects the horizontal $\tau = 0$ (black) line at $t = -T_w$.

Two-dimensional spectra were derived from time-domain signals such as in Fig. 2(b) by a 2D Fourier transform along τ and t . In Figs. 2(c) and 2(d), we show contour plots of the amplitude $|E_{\text{NL}}(\nu_\tau, \nu_t)|$ for waiting times $T_w = 35$ fs and $T_w = 827$ fs. The position of the different signal peaks is determined by the respective interaction sequence with the THz fields [24]. We basically observe strong nonlinear signals in the spectral range of the driving pulses $15 \text{ THz} < \nu_t < 25 \text{ THz}$ and on the two-phonon resonances $\nu_t = 10 \text{ THz}$ (the circles). Concerning the excitation frequency ν_τ , we find significant nonlinear signals for $\nu_\tau = 0$, $\nu_\tau = -\nu_t$, and $\nu_\tau = +\nu_t$. There are no 2D signals from interactions with one-phonon resonances around $\nu_t = 5 \text{ THz}$ because of strong absorption in this frequency range.

The 2D signals at $\nu_t = 22 \text{ THz}$ originate mainly from field-induced interband tunneling of carriers and from interband two-photon absorption [8,29,30]. Because of the extremely large transition dipole between the valence and the conduction band ($d_{\text{cv}} = e \times 4 \text{ nm}$ [31,32], where e is the elementary charge), the interband Rabi frequency for THz electric fields of $E = 50 \text{ kV/cm}$ is $\Omega_{\text{Rabi}} = Ed_{\text{cv}}/\hbar = 3 \times 10^{13} \text{ s}^{-1}$, comparable to the THz carrier frequency. Thus, light-matter interaction is in the strongly nonperturbative regime, allowing for multiple interaction sequences even with the electric field of a single THz transient.

We now analyze the two-phonon 2D signals occurring at $\nu_t = 10 \text{ THz}$. A Gaussian filter centered at the individual frequency vector (ν_τ, ν_t) is applied to the data, which are then Fourier back transformed into the time domain (τ, t) [23]. The results shown in Figs. 3(a) and 3(b) reveal the markedly different time structure of the signals at the (0, 10) and (10, 10) THz frequency positions. Comparing Figs. 3(a) and 3(c), one can see that the signal amplitude is independent of the coherence time τ . This behavior is due to interaction sequences in which a single THz pulse creates the oscillating two-phonon coherence. For closer inspection, we plot in Fig. 4(a) the two nonlinear transients $E_{\text{NL}}(t - T_w)$ (coherence time, $\tau = 0$). The red curve ($T_w = 827$ fs) is the direct continuation in amplitude and phase of the black transient for $T_w = 35$ fs. This agrees with the picture that pulse B creates the oscillating two-phonon coherence readout by pulse C. The signal field is radiated after pulse C and follows a free induction decay. The blue line in Fig. 4(a) is a fit of the amplitude decay with a time constant of $\tau_{\text{decay}} = 450$ fs corresponding to a linewidth of $\Delta\nu = 1.1 \text{ THz}$ (37 cm^{-1}). This value matches perfectly the 2TO-phonon density of states (Fig. 3 of Ref. [22]) but is $\approx\sqrt{2}$ times broader than the IR absorption (Fig. 2 of Ref. [20]), as will be discussed below. The two-phonon signal shown in Fig. 3(b) displays phase fronts perpendicular to those of pulse A, and thus it represents a rephasing signal. Its evolution as a function of the real time t [Fig. 4(b)] is similar to the transients in Fig. 4(a).

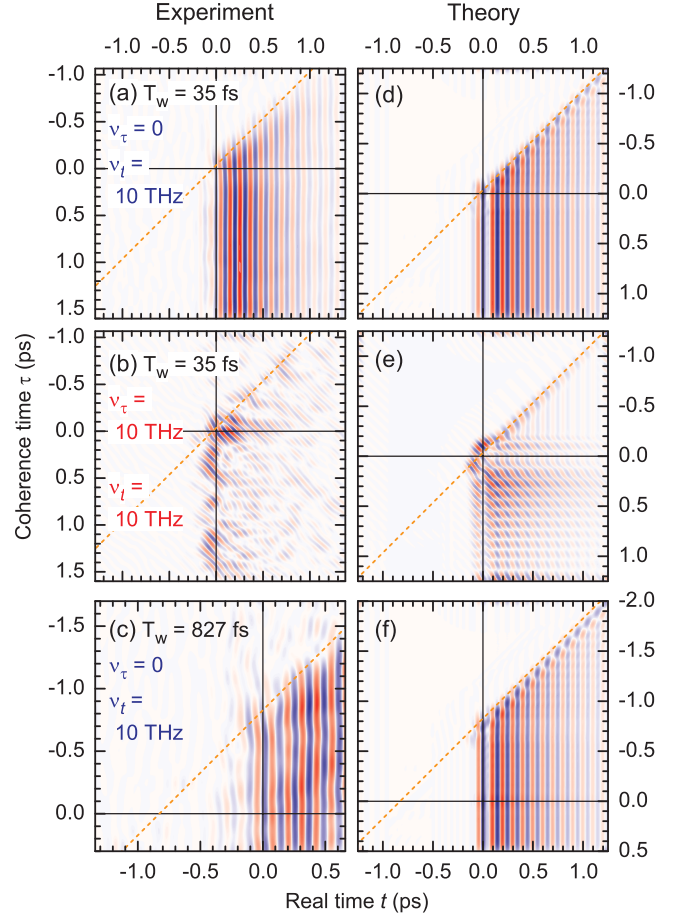


FIG. 3. Experimental time-domain 2D signals on different two-phonon peaks for waiting times of (a),(b) $T_w = 35$ fs and (c) $T_w = 827$ fs. (d)–(f) Calculated time-domain 2D signals.

We now discuss the light-matter interaction sequences relevant for the two-phonon coherences by considering Liouville pathways in the framework of density matrix theory. In Figs. 4(c)–4(f), pathways of different orders in the electric field, i.e., with different numbers of interactions, are illustrated using the diagrammatic technique of Ref. [33]. The linear response of the two-phonon coherence, the midinfrared absorption at 10 THz [20,21], is described by diagram Fig. 4(c). The absorption strength is proportional to $N_{\text{InSb}}|d_{2\text{ph}}|^2$ with the density of oscillators N_{InSb} and their transition dipole moment $d_{2\text{ph}}$ [34]. From the 2TO phonon absorption strength [20], one derives an extremely small transition dipole of $d_{2\text{ph}} = e \times 27 \text{ fm}$, resulting in a negligible linear contribution to the two-phonon coherences we observed.

Owing to its lack of inversion symmetry, the zinc blende structure possesses nonlinear susceptibilities $\chi^{(2)}, \chi^{(4)}, \dots$ of an even order. As a result, two-phonon coherences can, in principle, be generated by two-phonon-resonant difference frequency mixing [35]. However, the nonlinear 2D signal $E_{\text{NL}}(\tau, T_w, t)$ of Figs. 2–4 does not contain any $\chi^{(2)}$ contributions since, according to Eq. (1), only terms caused

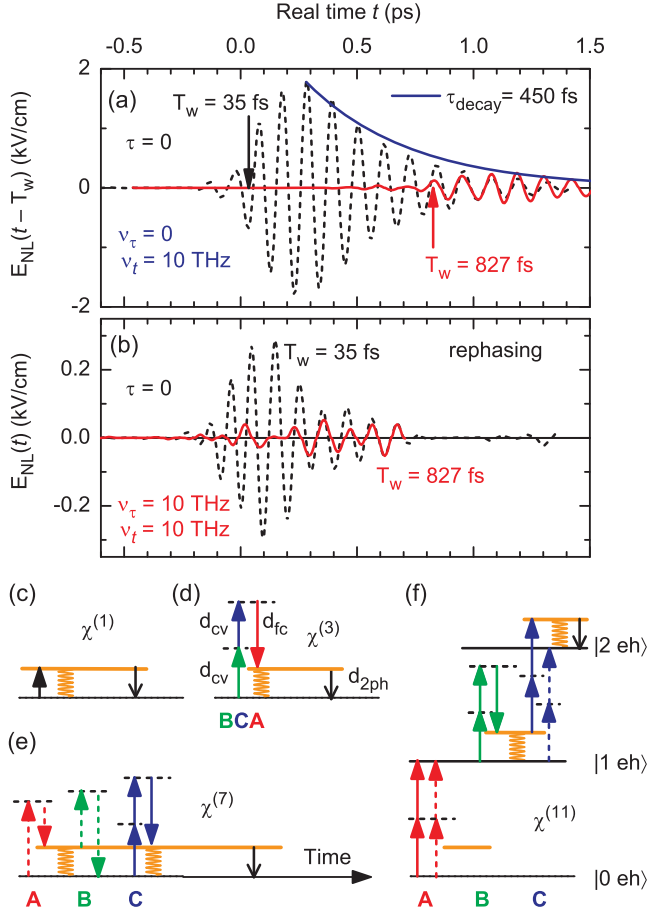


FIG. 4. (a) For a better comparison of the nonlinear transients from Figs. 3(a) and 3(c) at two different waiting times, we plot them here at $\tau = 0$ shifted in time by T_w . (b) Rephasing nonlinear transients at $\tau = 0$ [Fig. 3(b)]. (c)–(g) Liouville pathway diagrams of the relevant linear and nonlinear signal contributions. The arrows indicate possible pathways (time evolves from left to right). Evolutions on the $|ket\rangle$ and $\langle bra|$ side of the density matrix are displayed as solid and dashed arrows, respectively [33]. The final (black) arrow indicates the electric field emitted by the coherent polarization. The orange wavy lines indicate two-phonon coherences.

by all three interacting fields are preserved. Furthermore, in our experimental geometry with a (100)-oriented InSb crystal and collinearly polarized driving fields, all even-order contributions are excluded by the selection rules of point group $\bar{4}3m$, which require that the driving fields and the emitted field have finite projections onto all crystal axes [36] (nonzero components are, e.g., $\chi_{xyz}^{(2)}$, $\chi_{xyzz}^{(4)}$, and $\chi_{xyyyzzz}^{(6)}$).

We now address the rephasing nonlinear response at 10 THz [Figs. 3(b) and 4(b)]. The lowest-order diagram generating a rephasing two-phonon coherence is the $\chi^{(3)}$ process shown in Fig. 4(d). For all transitions off-resonantly driven by pulses A, B, and C, the rephasing nonlinear signal in Fig. 3(b) is strongest during the

(approximate) temporal overlap of all three pulses, i.e., at $T_w = 35$ fs and $\tau = 0$ [the dashed line in Fig. 4(b)]. In contrast to the linear absorption [Fig. 4(c)], which is proportional to $|d_{2ph}|^2$, this $\chi^{(3)}$ response involves the weak transition dipole d_{2ph} just once (during the emission of the signal field), so the $\chi^{(3)}$ response has a larger spectral width than the linear absorption.

The transition dipoles d_{cv} and d_{fc} result from electronic inter- and/or intraband transitions, relevant also to the two-photon absorption in InSb [29,30]. The nature of diagram Fig. 4(d) is similar to that of the ground state bleaching contribution in two-photon absorption but with modified transition dipoles. From the InSb Raman spectrum [22], one estimates the dipole moment $d_{fc} \approx 0.1 d_{cv} = e \times 0.4$ nm. Taking the parameters of our experiment, i.e., electric field $E = 50$ kV/cm, pulse duration $\Delta t = 200$ fs, and detuning $\hbar\Delta\omega \approx 10$ THz, we get a two-phonon coherence in the density matrix of $p_{2ph}^{(3)} \approx (d_{cv}E/\hbar\Delta\omega)^2 d_{fc}E\Delta t/\hbar = 0.1$ compared to $p_{2ph}^{(1)} \approx d_{2ph}E\Delta t/\hbar = 4 \times 10^{-5}$ in the linear case [Fig. 4(c)]. Thus, the nonlinear excitation scheme involving combined electronic and vibronic transitions generates two-phonon coherences orders of magnitude stronger than in the linear case. Since the driving pulses A, B, and C are off resonant, the rephasing nonlinear signal at $T_w = 827$ fs [the red curve in Fig. 4(b)] is much smaller. Here, only higher-order diagrams [cf. Fig. 4(e)] allow for a rephasing signal with a two-phonon coherence period between pulses A and B.

The nonrephasing signals in Figs. 3(a), 3(c), and 4(a) display vertical phase fronts. Since pulse A has diagonal phase fronts, it has to interact an even number of times (at least twice) to generate vertical phase fronts. According to Eq. (1), each of the pulses has to interact at least once. This rules out a $\chi^{(3)}$ process. The two-phonon coherence is created only by pulse B; it is independent of the pulse sequences ABC ($\tau > 0$), BAC ($-T_w < \tau < 0$), and BCA ($\tau < -T_w < 0$). In other words, the signal does not depend on the exact timing of pulses A and C. Thus, pulses A and C just create long-lived electronic excitations in InSb, requiring at least four interactions each. Figure 4(f) shows the lowest-order diagram that can lead to such a signal. For $\tau > 0$, pulse A performs a complete two-photon absorption event, thereby creating a first electron-hole pair. After the coherence time τ , pulse B creates the two-phonon coherence, which evolves during the waiting time T_w . Pulse C generates the second electron-hole pair, thereby transferring the two-phonon coherence (the orange wavy line) to the final electronic state. After the third pulse, the two-phonon coherence evolves along the real time t emitting radiation via its optical dipole (the black arrow). Similar Liouville pathways exist for the pulse sequences BAC and BCA.

Theoretical model calculations of the nonlinear two-phonon response are based on an ensemble of three-level

systems. The three levels are the ground state of the InSb crystal, an electronically excited state accessible by two-photon absorption—i.e., one electron-hole pair without two-phonon excitation—and the electronic ground state with the excitation of two TO phonons. The energy levels and decoherence times $T_2^{\text{interband}}$ and $T_2^{\text{two-phonon}}$ were adapted to experimental values and—for simplicity—infinite lifetimes of all levels were assumed. The calculated nonlinear response in Figs. 2(e) and 3(d)–3(f) is in excellent agreement with the data in Figs. 2(d) and 3(a)–3(c). In particular, the calculations reproduce the scenario in which a single pulse creates the oscillating two-phonon coherence, whereas the remaining two each perform a complete two-photon absorption event.

In conclusion, we have applied three-pulse 2D THz spectroscopy to map the dynamics of two-phonon coherences in a bulk semiconductor. In the nonperturbative limit of light-matter interaction, higher-order contributions in the driving fields strongly dominate over the linear two-phonon response. Our work paves the way towards 2D THz spectroscopy of low-energy excitations like phonons and magnons, and of transitions between ground and excited states of excitons and impurities with multiple-pulse sequences.

We acknowledge financial support by the Deutsche Forschungsgemeinschaft (Grant No. RE 806/9-1).

*woerner@mbi-berlin.de

- [1] Paul C. M. Planken, I. Brener, M. C. Nuss, M. S. C. Luo, and S. L. Chuang, Coherent control of terahertz charge oscillations in a coupled quantum well using phase-locked optical pulses, *Phys. Rev. B* **48**, 4903 (1993).
- [2] A. P. Heberle, J. J. Baumberg, and K. Köhler, Ultrafast Coherent Control and Destruction of Excitons in Quantum Wells, *Phys. Rev. Lett.* **75**, 2598 (1995).
- [3] R. Atanasov, A. Haché, J. L. P. Hughes, H. M. van Driel, and J. E. Sipe, Coherent Control of Photocurrent Generation in Bulk Semiconductors, *Phys. Rev. Lett.* **76**, 1703 (1996).
- [4] M. Woerner and J. Shah, Resonant Secondary Emission from Two-Dimensional Excitons: Femtosecond Time Evolution of the Coherence Properties, *Phys. Rev. Lett.* **81**, 4208 (1998).
- [5] T. Feurer, J. C. Vaughan, and K. A. Nelson, Spatiotemporal coherent control of lattice vibrational waves, *Science* **299**, 374 (2003).
- [6] M. Aeschlimann, M. Bauer, D. Bayer, T. Brixner, F. J. García de Abajo, W. Pfeiffer, M. Rohmer, C. Spindler, and F. Steeb, Adaptive subwavelength control of nano-optical fields, *Nature (London)* **446**, 301 (2007).
- [7] W. Kuehn, P. Gaal, K. Reimann, M. Woerner, T. Elsaesser, and R. Hey, Coherent Ballistic Motion of Electrons in a Periodic Potential, *Phys. Rev. Lett.* **104**, 146602 (2010).
- [8] W. Kuehn, P. Gaal, K. Reimann, M. Woerner, T. Elsaesser, and R. Hey, THz-induced interband tunneling of electrons in GaAs, *Phys. Rev. B* **82**, 075204 (2010).
- [9] W. Kuehn, K. Reimann, M. Woerner, T. Elsaesser, R. Hey, and U. Schade, Strong Correlation of Electronic and Lattice Excitations in GaAs/AlGaAs Semiconductor Quantum Wells Revealed by Two-Dimensional Terahertz Spectroscopy, *Phys. Rev. Lett.* **107**, 067401 (2011).
- [10] F. Junginger, B. Mayer, C. Schmidt, O. Schubert, S. Mährlein, A. Leitenstorfer, R. Huber, and A. Pashkin, Nonperturbative Interband Response of a Bulk InSb Semiconductor Driven Off Resonantly by Terahertz Electromagnetic Few-Cycle Pulses, *Phys. Rev. Lett.* **109**, 147403 (2012).
- [11] G. Folpini, D. Morrill, C. Somma, K. Reimann, M. Woerner, T. Elsaesser, and K. Biermann, Nonresonant coherent control: Intersubband excitations manipulated by a nonresonant terahertz pulse, *Phys. Rev. B* **92**, 085306 (2015).
- [12] H. Wang, K. Ferrio, D. G. Steel, Y. Z. Hu, R. Binder, and S. W. Koch, Transient Nonlinear Optical Response from Excitation Induced Dephasing in GaAs, *Phys. Rev. Lett.* **71**, 1261 (1993).
- [13] V. M. Axt and T. Kuhn, Femtosecond spectroscopy in semiconductors: A key to coherences, correlations and quantum kinetics, *Rep. Prog. Phys.* **67**, 433 (2004).
- [14] I. Waldmüller, J. Förstner, S.-C. Lee, A. Knorr, M. Woerner, K. Reimann, R. A. Kaindl, T. Elsaesser, R. Hey, and K. H. Ploog, Optical dephasing of coherent intersubband transitions in a quasi-two-dimensional electron gas, *Phys. Rev. B* **69**, 205307 (2004).
- [15] M. Artoni and J. L. Birman, Non-classical states in solids and detection, *Opt. Commun.* **104**, 319 (1994).
- [16] S. L. Johnson, P. Beaud, E. Vorobeva, C. J. Milne, É. D. Murray, S. Fahy, and G. Ingold, Directly Observing Squeezed Phonon States with Femtosecond X-Ray Diffraction, *Phys. Rev. Lett.* **102**, 175503 (2009).
- [17] J. Hu, O. V. Misochko, and K. G. Nakamura, Direct observation of two-phonon bound states in ZnTe, *Phys. Rev. B* **84**, 224304 (2011).
- [18] K. C. Lee, B. J. Sussman, M. R. Sprague, P. Michelberger, K. F. Reim, J. Nunn, N. K. Langford, P. J. Bustard, D. Jaksch, and I. A. Walmsley, Macroscopic non-classical states and terahertz quantum processing in room-temperature diamond, *Nat. Photonics* **6**, 41 (2012).
- [19] O. V. Misochko, Nonclassical states of lattice excitations: Squeezed and entangled phonons, *Usp. Fiz. Nauk* **183**, 917 (2013) [*Sov. Phys. Usp.* **56**, 868 (2013)].
- [20] S. J. Fray, F. A. Johnson, and R. H. Jones, Lattice absorption bands in indium antimonide, *Proc. Phys. Soc.* **76**, 939 (1960).
- [21] E. S. Koteles, W. R. Datars, and G. Dolling, Far-infrared phonon absorption in InSb, *Phys. Rev. B* **9**, 572 (1974).
- [22] W. Kiefer, W. Richter, and M. Cardona, Second-order Raman scattering in InSb, *Phys. Rev. B* **12**, 2346 (1975).
- [23] W. Kuehn, K. Reimann, M. Woerner, T. Elsaesser, and R. Hey, Two-dimensional terahertz correlation spectra of electronic excitations in semiconductor quantum wells, *J. Phys. Chem. B* **115**, 5448 (2011).
- [24] M. Woerner, W. Kuehn, P. Bowlan, K. Reimann, and T. Elsaesser, Ultrafast two-dimensional terahertz spectroscopy of elementary excitations in solids, *New J. Phys.* **15**, 025039 (2013).
- [25] Q. Wu and X.-C. Zhang, Free-space electro-optics sampling of mid-infrared pulses, *Appl. Phys. Lett.* **71**, 1285 (1997).

- [26] K. Reimann, R. P. Smith, A. M. Weiner, T. Elsaesser, and M. Woerner, Direct field-resolved detection of terahertz transients with amplitudes of megavolts per centimeter, *Opt. Lett.* **28**, 471 (2003).
- [27] G. W. Gobeli and H. Y. Fan, Infrared absorption and valence band in indium antimonide, *Phys. Rev.* **119**, 613 (1960).
- [28] C. L. Littler and D. G. Seiler, Temperature dependence of the energy gap of InSb using nonlinear optical techniques, *Appl. Phys. Lett.* **46**, 986 (1985).
- [29] C. R. Pidgeon, B. S. Wherrett, A. M. Johnston, J. Dempsey, and A. Miller, Two-Photon Absorption in Zinc-Blende Semiconductors, *Phys. Rev. Lett.* **42**, 1785 (1979); **43**, 1843(E) (1979).
- [30] A. Miller, A. Johnston, J. Dempsey, J. Smith, C. R. Pidgeon, and G. D. Holah, Two-photon absorption in InSb and $\text{Hg}_{1-x}\text{Cd}_x\text{Te}$, *J. Phys. C* **12**, 4839 (1979).
- [31] E. O. Kane, Zener tunneling in semiconductors, *J. Phys. Chem. Solids* **12**, 181 (1960).
- [32] E. O. Kane, Band structure of indium antimonide, *J. Phys. Chem. Solids* **1**, 249 (1957).
- [33] W. T. Pollard, S. L. Dexheimer, Q. Wang, L. A. Peteanu, C. V. Shank, and R. A. Mathies, Theory of dynamic absorption spectroscopy of nonstationary states. 4. Application to 12-fs resonant impulsive Raman spectroscopy of bacteriorhodopsin, *J. Phys. Chem.* **96**, 6147 (1992).
- [34] Because of the extremely flat dispersion of TO phonons in InSb [37], we consider here identical “anharmonic” TO oscillators with the density of InSb molecules in an InSb crystal.
- [35] C. Somma, G. Folpini, J. Gupta, K. Reimann, M. Woerner, and T. Elsaesser, Ultra-broadband terahertz pulses generated in the organic crystal DSTMS, *Opt. Lett.* **40**, 3404 (2015).
- [36] R. Fieschi, Matter tensors in the crystallographic groups of Cartesian symmetry, *Physica (Amsterdam)* **23**, 972 (1957).
- [37] D. L. Price, J. M. Rowe, and R. M. Nicklow, Lattice dynamics of grey tin and indium antimonide, *Phys. Rev. B* **3**, 1268 (1971).